INL/JOU-25-87393-Revision-0

Micro-tensile testing of neutron irradiated Al/Zr and Zr/U-Mo Diffusion Bonds

January 2026

Changing the World's Energy Future

Jason L Schulthess, Cameron Boyd Howard, Tanner Jason Mauseth, Christopher George Bearcroft

INL/JOU-25-87393-Revision-0

Micro-tensile testing of neutron irradiated Al/Zr and Zr/U-Mo Diffusion Bonds

Jason L Schulthess, Cameron Boyd Howard, Tanner Jason Mauseth, Christopher George Bearcroft

January 2026

Idaho National Laboratory
Idaho Falls, Idaho 83415

http://www.inl.gov

Prepared for the
U.S. Department of Energy
Under DOE Idaho Operations Office
Contract DE-AC07-05ID14517

Micro-tensile testing of neutron-irradiated Al/Zr and Zr/U-Mo diffusion bonds

Jason L. Schulthess[1, 2], Cameron B. Howard[1], Tanner J. Mauseth[1], Christopher Bearcroft[1]

Jason L. Schulthess, Jason.schulthess@inl.gov, ORCID: 0000-0002-4289-7528

Cameron B. Howard, Cameron.howard@inl.gov, ORCID: 0000-0001-5134-213x

Tanner J. Mauseth, tanner.mauseth@inl.gov, ORCID: 0000-0001-9574-0463

Christopher Bearcroft, Christopher.bearcroft@inl.gov, ORCID:

1) Idaho National Laboratory, 1955 N. Freemont Ave, Idaho Falls, Idaho, USA, 83415
2) Corresponding Author

Abstract

This study focuses on micro-tensile testing of neutron-irradiated Al/Zr and Zr/U-Mo diffusion bonds, which are integral to the structure and performance of nuclear fuel plates used in the fuel being developed for U.S. high-power research reactors. The fuel consists of uranium metal alloyed with 10 wt% molybdenum (U-10Mo), and diffusion bonded with zirconium and aluminum. Two distinct diffusion bonds occur—one at the Zr/U-10Mo interface via roll bonding, and the Zr/Al interface via hot isostatic pressing at 833 K. Understanding the post-irradiation mechanical behavior of these diffusion layers is critical to ensuring the fuel's stability and integrity. While previous studies have shown that U-10Mo loses ductility and becomes brittle due to irradiation-induced porosity, the mechanical properties of the diffusion layers remain largely unknown.

This work utilizes micro-tensile testing specimens approximately 7 × 7 × 20 μm^3, which are sufficiently large to encompass the identified diffusion zones to evaluate the failure strength and identify the failure location. For the Zr/Al interface, all failures occurred in the bulk aluminum. The average yield strength, ultimate strength, and strain at failure for the two parent samples were: 125 ± 10 MPa, 139 ± 24 MPa, 156 ± 21 MPa, 185 ± 14 MPa, 37.9 ± 5.6%, and 29.7 ± 3.4%, respectively. For specimens across the Zr/U-Mo interface, failures occurred either in the bulk Zr or U-Mo, with no failures observed in the diffusion region.

These findings support the development of accurate thermo-mechanical models for irradiated fuel performance by identifying the mechanical limits and failure locations within the bonded regions.

Introduction

High-power research nuclear reactors in the United States (U.S.) serve critical roles in nuclear isotope production, material testing and fuels development. These reactors currently utilize highly enriched uranium (HEU) containing over 90% of the fissile isotope ^{235}U raising nuclear proliferation concerns. To mitigate this risk while maintaining reactor performance, a new low enriched uranium (LEU) fuel is being developed containing less than 20% ^{235}U [1, 2].

In this new fuel design, uranium metal is alloyed with 10 wt% molybdenum (U-10Mo) and rolled into thin foils. During rolling, a zirconium (Zr) layer is diffusion bonded to the U-10Mo. The resulting foil is encapsulated in aluminum (Al) using hot isostatic pressing (HIP) at 833 K, forming a multi-layer plate consisting of fuel, interlayer and cladding [1, 3, 4]. Figure 1 shows a schematic cross section of the monolithic fuel plate with a U-10Mo core, a Zr layer on either side, encapsulated in Al cladding. While the schematic exposes the fuel edges to highlight the diffusion interfaces, in practice, the fuel is fully encapsulated in Al to prevent fission product release into the reactor coolant.

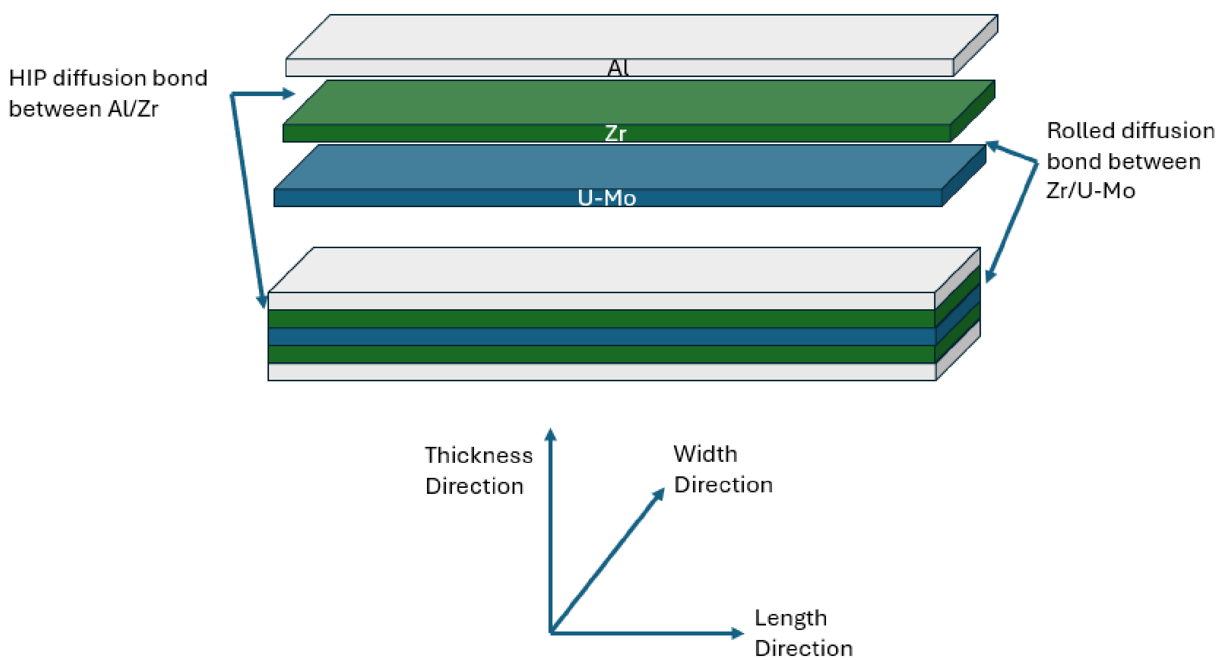

Figure 1. Cross-sectional schematic of monolithic fuel plate architecture, location of rolled diffusion bond between Zr and U-Mo, and the HIP diffusion bond between Al/Zr.

The two diffusion-bonding processes result in complex interdiffusion zones, one at the U-10Mo/Zr interface (roll-bonded interface) and another at the Zr/Al interface (HIP-bonded interface). The formation and growth of the resulting diffusion layers have been previously characterized [5-7] However, these zones' mechanical behavior under neutron irradiation is poorly understood. A schematic representation (not to scale) of the diffusion layers formed at the interfaces is shown in Figure 2.

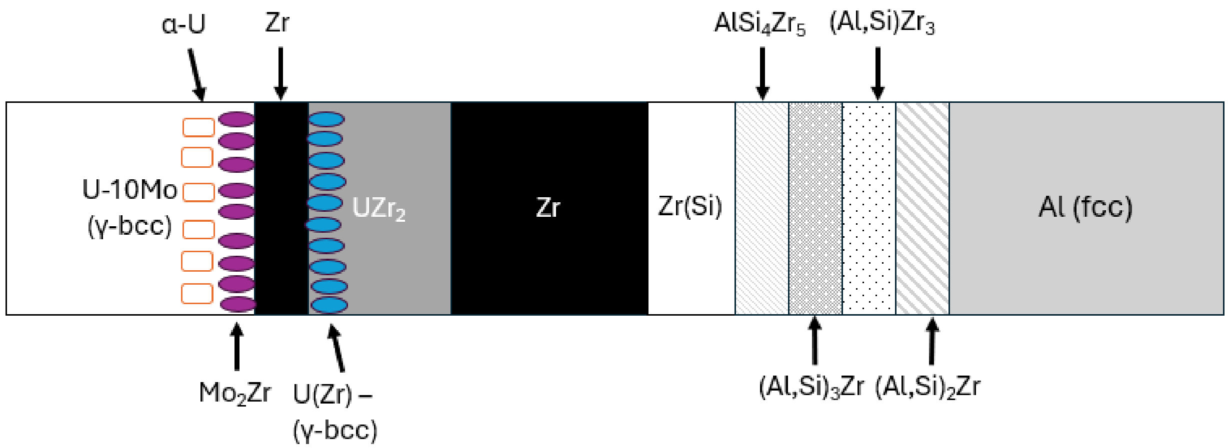

Figure 2. Zr/U-10Mo and Zr/Al interdiffusion zones resulting from diffusion-bonding fabrication process steps [5, 7].

Understanding the mechanical behavior of these interdiffusion zones is necessary to ensure the fuel maintains geometric stability, mechanical integrity, and stable and predictable behavior during irradiation as failure of these layers could result in undercooling by delamination, or excessive plate deformation via closing of coolant channels [8]. Figure 3 provides previous optical microscopy of the interfaces from [9], demonstrating that the layers remain well bonded up to very high fission densities (9.5×10^{27} f/m^3), where the bubbles appear to concentrate and interconnect in the α-U zone adjacent to the U-10Mo / Zr interface.

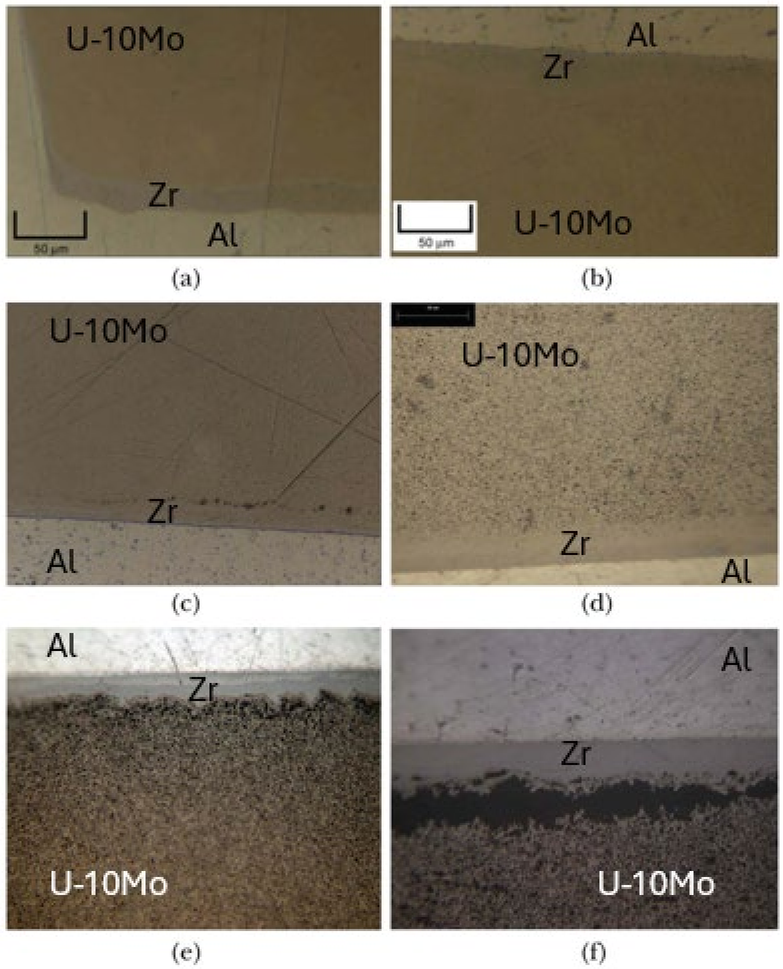

Figure 3. Optical microscopy images of the U-10Mo/Zr and Zr/Al interfaces at different fuel burnup / fission density levels (10^{21} f/cm^3). (a) 2.2, (b) 4.0, (c) 6.2, (d) 7.2, (e) 8.4, (f) 9.5, reproduced from [9].

While failure at high burnup may intuitively occur in the fuel, behavior at intermediate burnups is less predictable due to competing factors influencing the mechanical properties. For example, Farrell [10-13] showed that irradiation-induced hardening can occur in aluminum 6061 alloys, beginning with thermal fluences near 10^{25} n/m^2 and fast fluences (E>0.1 MeV) above 10^{23} n/m^2. The extent of hardening was shown to depend on the ratio of the thermal to fast neutron flux ($Flux_{Th}/Flux_F$). Additionally, U-10Mo loses its ductility and becomes brittle due to the development of porosity as burnup increases [14-17].

Despite these results, the mechanical properties of the diffusion layers remain largely unknown due to the challenges of performing mechanical tests on irradiated materials. These properties are necessary for developing accurate thermo-mechanical models to predict fuel performance over a range of irradiation conditions. Existing models evaluate the stresses, strains, and deformations during irradiation, which are dependent on material properties but are limited due to unknown characteristics of the interdiffusion layers and the integrity of the diffusion bond as irradiation burnup increases [18-22].

Given the small scale of the diffusion zones and the need to assess interfacial strength post-irradiation, micro-mechanical testing techniques are required. While micro-cantilever testing has been used to evaluate U-Mo foils [23]. Its geometry is not well-suited for probing diffusion interfaces. Instead, micro-tensile samples have been developed and have been used to evaluate the Al/Al bond in these nuclear fuel plates along with the bulk and interfacial properties in tri-structural isotopic (TRISO) architecture fuels [24, 25]. In these prior works, micro-tensile specimens with tensile gauge dimensions of approximately 7 × 7 × 20 μm^3 have been successfully demonstrated. This size sample is sufficiently large to be larger than the interdiffusion zone of either interface previously identified by Perez et al. [7]. As a result, an integral tensile test of both the bulk and diffusion zones between the Al/Zr and Zr/U-Mo interfaces is expected from this work to allow identification of the failure location (diffusion zone or bulk) and the failure strength.

Materials and Methods

Material for this study was derived from the Advanced Test Reactor-Full size plate-In the center flux trap Position (AFIP)-7 irradiation experiment, hereafter referred to as AFIP-7. The experiment included four full-size fuel plates fabricated using the process described in the introduction. The four plates were irradiated for two cycles in the Advanced Test Reactor (ATR) at Idaho National Laboratory (INL). Each fuel plate had a U-10Mo fuel meat of approximately 330 μm thick and a Zr layer of approximately 25 μm, all clad in AL6061 cladding.

Samples were selected from the fuel plate ZH2 which was previously reported with irradiation conditions and post-irradiation examinations. The peak burnup of plate ZH2 was 41.5% ^{235}U burnup corresponding to a peak fission density of 2.96 × 10^{21} fissions/cm^3. The plate average burnup was reported as 32.9% ^{235}U burnup corresponding to an average fission density of 2.32 × 10^{21} fissions/cm^3 [26-30].

Two samples were sectioned from the bottom region of the fuel plate:

Mount 73Y, with an estimated fission density of 1.69 × 10^{21} fissions/cm^3, a local thermal neutron fluence of 5.73 × 10^{21} n/cm^2 and a surface temperature of the aluminum approximately 337 K.

Mount 72Y, located approximately 7 cm from the bottom of the fuel zone with a local fission density of 2.0 × 10^{21} fissions/cm^3, thermal neutron fluence of 6.44 × 10^{21} n/cm^2, and an estimated surface temperature of 347 K [28, 29].

These samples were chosen to represent intermediate burnup conditions, with microstructures similar to those shown in Figure 3a. Additionally, the neutron fluences are below the threshold identified by Farrell for appreciable Al to Si transmutation so the effects of Si incorporation into the Al matrix will be neglected [11].

The micro-tensile specimens were fabricated from the bulk material using a shielded Plasma Focused Ion Beam (PFIB) Scanning Electron Microscope (SEM) Dual Beam coupled with Energy Dispersive Spectroscopy (EDS). The equipment, a ThermoFisher Helios Generation 3 PFIB SEM, is installed in a shielded enclosure in the Irradiated Materials Characterization Laboratory (IMCL) at

INL, which allows for handling and analysis of irradiated nuclear fuels. Sample preparation followed an in-plane style lift-out method developed by Mauseth et al. [25]. This ensures sufficient volumes were obtained to embed lifted-out blocks of the material into molybdenum substrate grids so that the interface of interest remained approximately within the center of the gauge. The sample design also helps ensure that deformation during the tensile test occurs in the gauge region by employing quarter-circle radius patterns that allow smooth transitions from the gauge region to the head region to minimize stress concentrations at the specimen shoulders. Figure 4 shows representative specimens from the Zr/Al interface of sample 72Y with 7 × 7 × 18 μm^3 gauge dimensions.

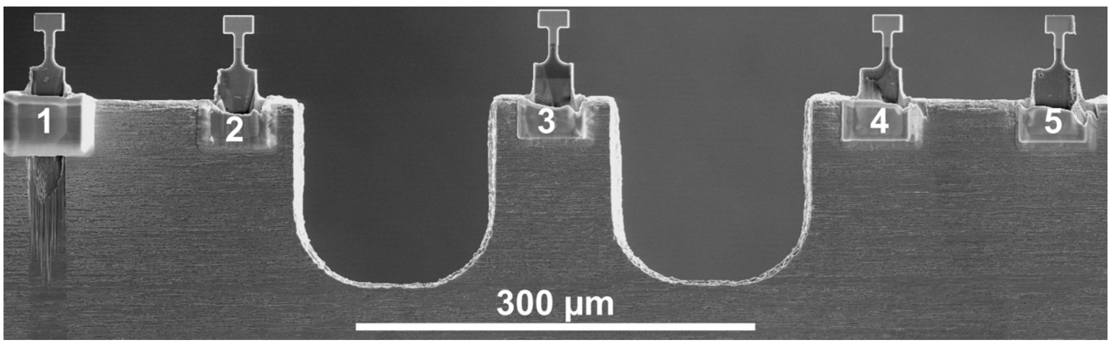

Figure 4. Representative batch of 7 × 7 × 18 μm^3 gauge dimension tensile specimens prepared from the Zr/Al interface from specimen 72Y. The plate fuel sample is from approximately 7 cm from the bottom of the fuel plate with local fission density and thermal neutron fluence of 2.0×10^{21} fissions/cm^3, and 6.44×10^{21} n/cm^2, respectively.

A Bruker Hysitron 20 µm flat punch diamond indentation probe was modified into the gripper that pulled the free end of the tensile specimens shown in Figure 9. This gripper was made using the oxygen plasma on the Generation 4 PFIB to mill out a reverse-T shape with smooth, well aligned edges that meet the T-shaped tensile heads. Tensile testing was conducted in an SEM using a PI88 Pico-indenter, which was programmed to apply tensile rather than compression to put the samples under tension.

The modified gripper, fabricated from the indentation probe, was mounted to the transducer's threaded posts, and the PI 88's stage was used to align each specimen within the gripper. To verify alignment, a touch test was performed by pulling on the gripper/specimen until a load of 1 to 2 µN was achieved. If necessary, realignments were made until a successful touch test was achieved.

Once alignment was confirmed, tensile testing was performed using a constant displacement rate of approximately 18 nm/s corresponding to a strain rate of approximately 10^{-3}strain/s, until the specimen failed. During testing, in situ SEM images were captured and later analyzed using Digital Image Correlation software to calculate the strain for each test.

Prior to each test, each specimen was analyzed via SEM-EDS. This analysis confirmed the location of the bond interface to be in the gauge region and provided confirmation of the diffusion gradient at the interface.

SEM-EDS Results

Area SEM-EDS maps in Figure 5 show a single tensile specimen from the Zr/U-Mo region of sample 73Y. The figure highlights the critical elements of interest, including U, Mo, Zr, and Si. A Mo-rich layer with thickness approximately 1.192 ± 0.351 µm is present at the interface and is likely the Mo_2Zr layer previously identified by Perez et al. [6, 7]. Other layers identified by Perez are not distinguishable at this magnification. All other Zr/U-Mo tensile specimens from both parent samples show similar results from the SEM-EDS analysis, including the presence of the approximately 1-µm Mo-rich layer. Figure 6 shows the SEM-EDS map of the Zr/Al interface with elements Al, Zr, and Si highlighted. A Si-rich layer is revealed at the interface that is approximately 1.345 µm in thickness. This is similar to the results previously shown for this interface by Perez et al. However, the nm-sized layers identified by Perez et al. are not distinguishable at this magnification [6, 7]. All other Zr/Al interface tensile specimens from both parent samples show similar results from the SEM-EDS analysis, including the presence of the approximately 1.3-µm-thick Si-enriched zone at the interface. In Figures 5 and 6, the elemental intensity maps represent net counts of the element of interest above background.

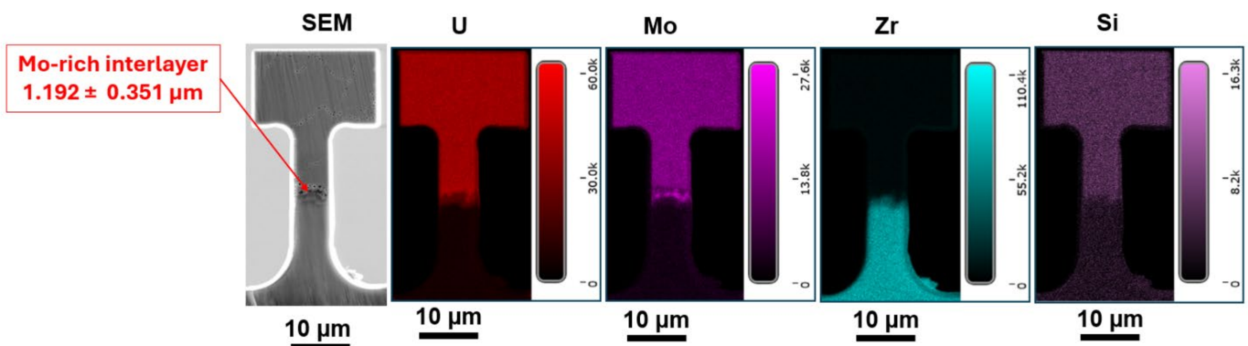

Figure 5. SEM-EDS area map of a single tensile specimen from sample 73Y with local fission density estimated to be 1.69×10^{21} fissions/cm^3. The local thermal neutron fluence is estimated to be 5.73×10^{21} n/cm^2. Net counts of elements U, Mo, Zr, and Si are shown.

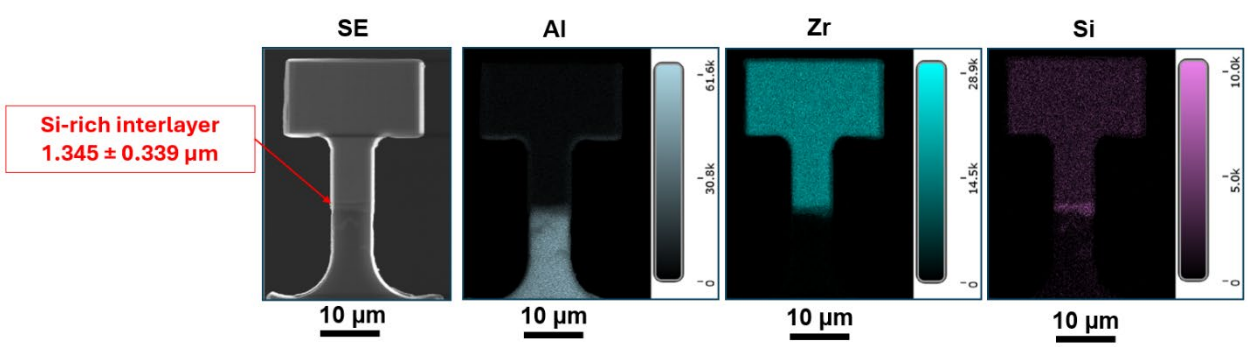

Figure 6. SEM-EDS area map of a single tensile specimen from sample 72Y with local fission density estimated to be 2.0×10^{21} fissions/cm^3, and the local thermal neutron fluence estimated to be 6.44×10^{21} n/cm^2. Net counts of elements Al, Zr, and Si are shown.

Zr/Al Interface Tensile Test Results

A total of nine tensile specimens from the Zr/Al interface were successfully tested. All specimens failed within the bulk aluminum, away from the diffusion bonded interface, indicating that the interface itself remained mechanically robust under the tested conditions.

Table 1 summarizes the mechanical properties of the specimens including the 0.2% offset yield stress, ultimate tensile stress (UTS), and the strain at failure. Although this material has a different thermal history than AA6061-O temper, the expected properties of poly-crystalline O temper are included for reference [31].

Table 1. Mechanical properties summary of Zr/Al tensile specimens.

Sample	**σ_y [MPa]**	**σ_{UTS} [MPa]**	**ε_{total} [%]**
Non-Irradiated AA6061-O [31]	83 – 110	150	10 – 18
72Y	125 ± 10	156 ± 21	37.9 ± 5.6
73Y	139 ± 24	185 ± 14	29.7 ± 3.4

Engineering stress and strain curves for the five specimens tested from sample 72Y are shown in Figure 7. Similarly shaped curves were found for the specimens tested from sample 73Y, but are not shown for brevity, and clarity on the figure. However, the stress and strain curves from sample 73Y of the Zr/Al interface can be seen in Figure 1 of the supplementary materials.

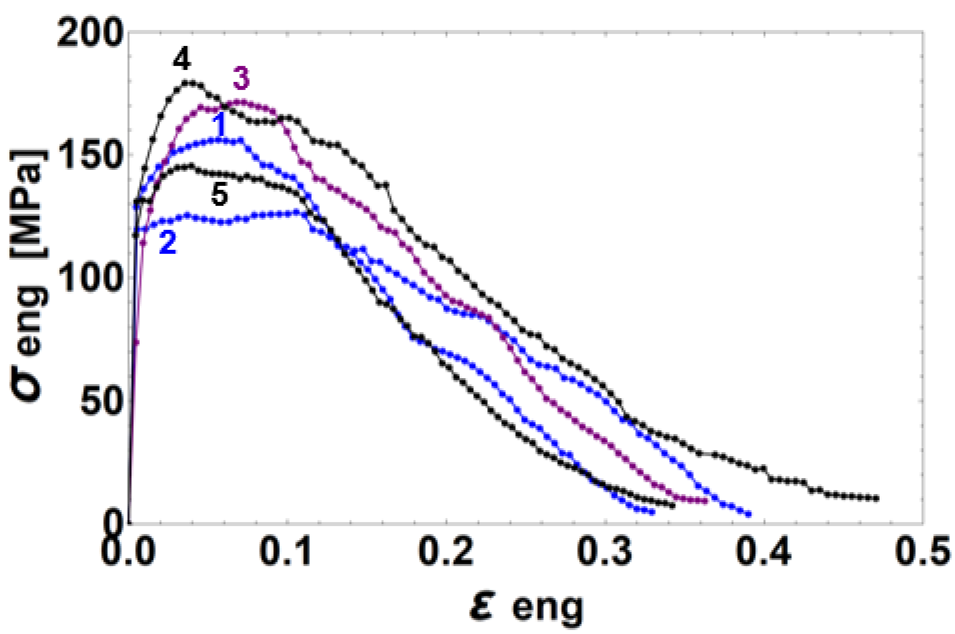

Figure 7. Stress and strain curves for the five specimens tested from sample 72Y containing the Zr/Al interface. Specimens 1 and 2 (blue) exhibit slip steps that appear entirely within the Al phase of the gauge and plastically deform to failure. Specimen 3 (magenta) exhibits a slip step that first develops at the intersection of the Si-rich interface and the Al phase on the right side of the gauge at the free surface. (See also Figure 8.) Specimens 4 and 5 plastically deform entirely in the Al phase in

a more homogeneous way. Distinct slip bands are less evident, and necking behavior is observed in the Al phase of the gauge as it plastically deforms to failure.

Zr/U-Mo Interface Tensile Test Results

Ten Zr/U-Mo tensile specimens were successfully fabricated and tested between the two parent samples. Two distinct failure modes were detected. Six specimens fractured in the U-Mo portion of the gauge, and four yielded and plastically deformed to failure in the Zr portion of the gauge. Due to the differing failure modes, results are subdivided by parent sample and failure mode. The modulus, ultimate tensile stress, and total elongation are provided in Table 2.

Table 2. Mechanical properties summary of Zr/U-Mo tensile specimens.

Sample		E [GPa]	$\sigma_{failure}$ [MPa]	ε_{total} [%]
72Y	Fuel Failure	121 ± 30	596 ± 32	2.2 ± 1.3
	Zr Plasticity	123	570	43.3
73Y	Fuel Failure	76 ± 10	548 ± 124	1.5 ± 0.6
	Zr Plasticity	83 ± 17	710 ± 131	27.3 ± 6.6

Stress and strain curves from the Zr/U-Mo tensile samples are shown in Figure 8. Green curves show the tensile specimens, which failed in the U-Mo portion of the gauge while the blue curves show those that failed in the Zr portion of the gauge. The extended tail after yielding of the blue curves is indicative of the plastic deformation that occurred.

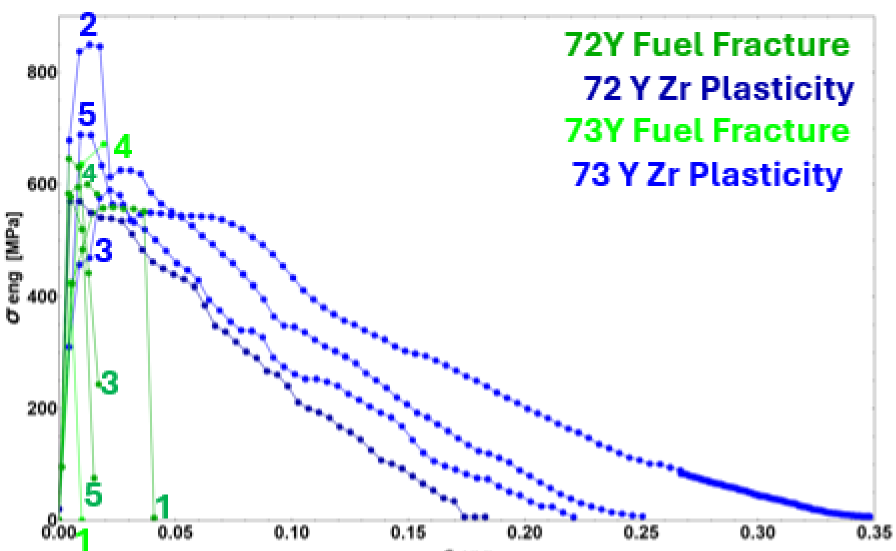

Figure 8. Stress and strain curves from the Zr/U-Mo tensile specimens from samples 72Y and 73Y. The green curves represent the specimens that failed in the U-Mo portion of the gauge, while the blue curves show the specimens that plastically deformed and failed in the Zr portion.

Because several of the specimens failed in a brittle manner in the U-Mo portion of the gauge, the ultimate tensile strength of those samples is provided in Table 3.

Table 3. 72Y and 73Y Zr/U-Mo fuel failure ultimate tensile strength values.

Sample and Specimen ID	Ultimate Tensile Strength (MPa)
72Y, Tensile Bar 1	559
72Y, Tensile Bar 3	646
72Y, Tensile Bar 4	600
72Y, Tensile Bar 5	580
73Y, Tensile Bar 1	424
73Y, Tensile Bar 4	672
Average	580 ± 87

Discussion

Zr/Al Interface

All nine tensile specimens failed within the bulk aluminum, rather than at the diffusion bonded interface. Therefore, we can qualitatively conclude that the diffusion bond is stronger than the bulk aluminum and is stronger than the ultimate tensile strength measured for the bulk aluminum of 156 ± 21 MPa and 185 ± 14 MPa for samples 72Y and 73Y, respectively. High-resolution SEM test videos revealed subtle differences in the deformation behavior between the individual tests. Four specimens showed distinct slip steps entirely in the Al gauge portions. Three specimens showed homogeneous plastic deformation and necking behavior in the Al regions. Two specimens initiated slip where the Si-rich interface, Al region, and free surface intersect. In these two cases, the slip propagates further into the Al regions of the gauges and further plasticity causes failure in the Al regions of the gauges. These subtle differences may be attributed to differences in crystallographic orientation of the grains in the Al region. Figure 8 shows examples of where the first deformation is identified from the video during the tensile tests of two specimens from sample 72Y.

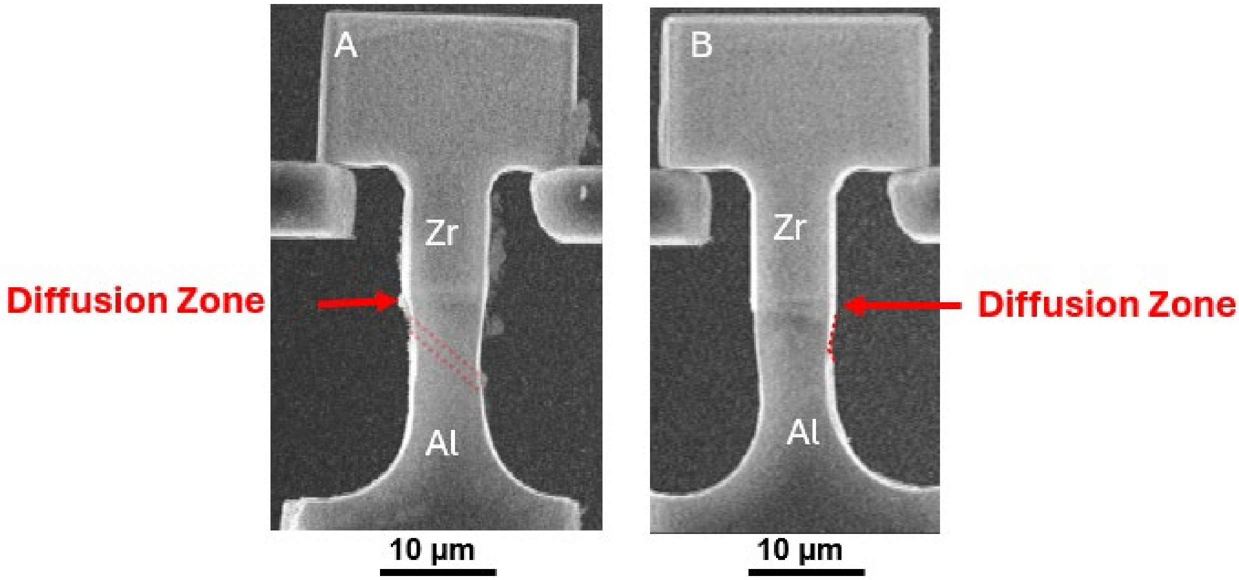

Figure 9. Example of first slip bands and deformation visible in Zr/Al tensile specimens from sample 72Y. A) The first visible slip bands are highlighted and appear entirely in the aluminum. B) The first deformation occurs at the interface of the bulk aluminum and Si-enriched diffusion zone, but the deformation propagates to the bulk aluminum where the specimen eventually fails.

It is known that the Al portion of the cladding is similar to the AA6061-O temper, but that it does not match exactly [8] due to the HIP process being performed at 833 K, which exceeds the AA6061 solution temperature of approximately 800 K [32]. Previous work [8], reports that the unirradiated yield strength of the HIP-bonded Al is between 66–72 MPa, with the ultimate tensile strength being between 141–144 MPa, and the total elongation between 22%–26%. The yield strengths of the Zr/Al samples, noting that all the samples deformed and failed in the Al portion of the gauge, have higher yield strengths and total elongation compared to the unirradiated O temper, but have similar ultimate tensile strengths. The longer elongation values in the micro-tensile specimens may be due to sampling a single grain, or too few grains compared to a bulk polycrystalline test. Additionally, while the small size of the samples is known to be a contributing factor [33-35], the fluence and irradiation temperature are also considered. In this case, sample 73Y had a lower fluence and irradiation temperature compared to 72Y. The fluence and temperature for 73Y was 5.73×10^{21} n/cm^2 and approximately 337 K while for 72Y it was 6.44×10^{21} n/cm^2 and approximately 347 K. The slightly lower irradiation temperature of 73Y may have led to less annealing of point defect damage and the resulting higher yield strength, ultimate strength, and lower elongation compared to 72Y.

Discussion Zr/U-Mo Interfaces

All ten Zr/U-Mo tensile specimens failed outside the diffusion zone. Figure 10 shows representative images of tensile specimens from sample 73Y, which failed either in the U-Mo or Zr portions of the gauge region. The consistent failure behavior indicates that at this intermediate burnup, the diffusion zone is mechanically stronger than the surrounding bulk material. Specifically, it withstood stresses exceeding the lowest recorded failure stress of approximately 570 MPa (bulk Zr failure), suggesting a robust interfacial bond. Consistent with the differences in failure mode, the total strain for individual specimens was either in the 2% range for specimens that failed in the U-Mo by brittle failure or was greater than 27% for those that failed in the Zr portion of the gauge. At this intermediate burnup, some porosity is beginning to be visible in the Mo-depleted region near the diffusion zone (see Figure 10). Yet, this concentration of bubbles was not the failure location, meaning that these features are not yet large enough to dominate the ultimate strength.

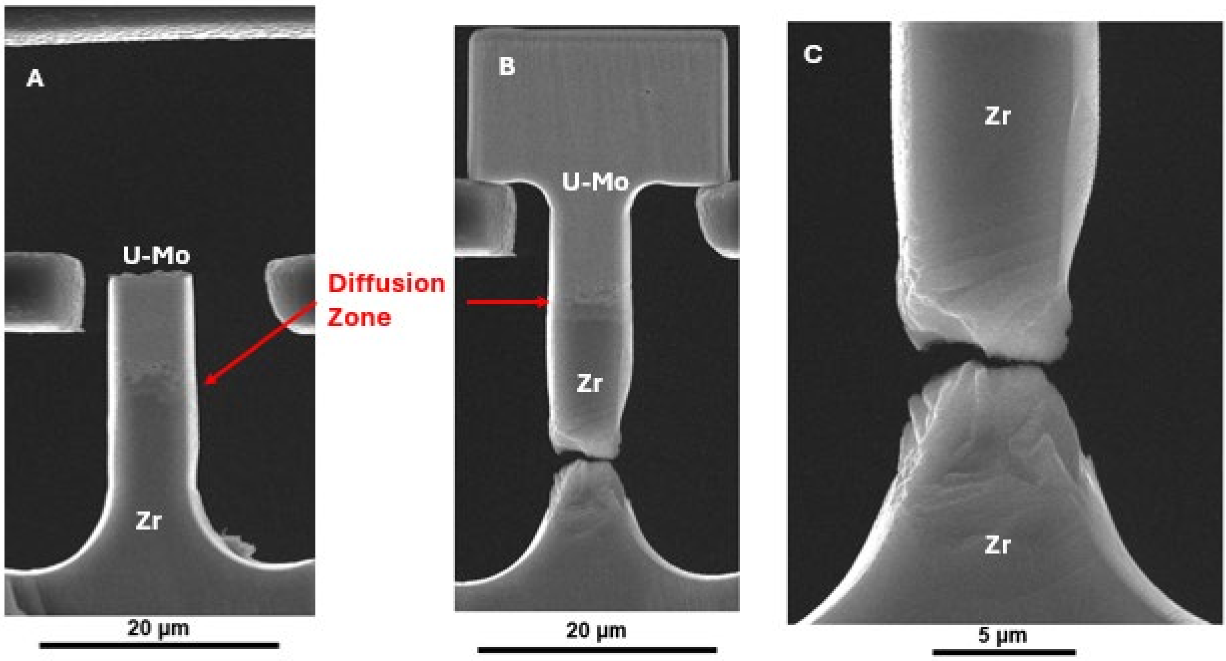

Figure 10. Example of Zr/U-Mo interface tensile specimens after failure from sample 73Y. The diffusion zone between the U-Mo and Zr regions of the gauge is visible. A) Tensile specimen 1, brittle fracture entirely in the U-Mo portion of the gauge. B) Tensile specimen 2, ductile fracture entirely in the Zr portion of the gauge. C) Magnified image of necking and fracture location of tensile specimen 2 from sample 73Y. The reduction of area is visible in images B and C, but there is no evidence of reduction of area in A.

Because several of the specimens failed in the U-Mo portion of the gauge, comparison to prior studies is possible. Bulk-scale tensile tests of unirradiated and rolled U-Mo alloy foil with similar fabrication history to the material investigated in this work report approximate modulus, yield strength, ultimate tensile strength and elongation are 82.4 GPa, 933 MPa, 935 MPa, and 9.5%, respectively [14, 15, 36]. Bend tests of irradiated U-Mo foils, again with similar fabrication history, and similar burnup to the material investigated in this work (2.05×10^{21} fissions/cm^3) show that the modulus and bending strength are approximately 68.2 GPa and 214.5 MPa, respectively [16, 17]. For the case of specimens from sample 72Y, which failed in the U-Mo, the modulus was measured to be approximately 121 ± 30 GPa, which is larger than either prior set of experiments on bulk-scale material. At present, it is not understood why the modulus values from sample 72Y are larger than expected, especially since, as will be discussed later, the modulus values from sample 73Y are reasonably consistent with prior literature.

The failure strength of the micro-tensile irradiated U-Mo (596 ± 32 MPa) is lower than the fresh, unirradiated U-Mo tensile tests (933 MPa). This difference may be indicative of the rapid degradation of strength due to both fission damage and development of porosity in the fuel. However, at 596 ± 32 MPa the micro-tensile irradiated U-Mo failure strength is larger than that measured by bulk four-point bend testing (214.5 MPa). The ratio of the bending strength to the tensile strength at similar fission density is 2.79. This is remarkably close to the bending to tensile strength ratio previously developed by Schulthess et al., based on the methodology of Leguillon et al., where the Weibull Modulus is used as a scaling parameter. In this prior work, the Leguillon ratio was found to be 2.687 [16, 37]. This indicates that the strength of the U-Mo in this work is consistent with the bulk strengths of U-Mo found in prior literature.

For the specimens from 73Y, the modulus is 76 ± 10 GPa, which is consistent with prior literature results of irradiated U-Mo foils at similar burnup which found the modulus to be 68.2 GPa. Given the uncertainties of experimental mechanical testing, the results of this work for modulus (76 GPa) are reasonably similar. The strength values for 73Y for the U-Mo failed samples are similar to those from 72Y of 548 ± 124 MPa. As with specimens from 72Y, this strength value is lower than was found in unirradiated tensile specimens of U-Mo rolled foils, indicating the rapid degradation of strength due to both fission damage and development of porosity in the fuel.

For the specimen from sample 72Y, which failed in the Zr, the modulus (123 GPa) is larger than expected in available literature for bulk alpha Zr (93 GPa) [38]. However, the modulus results from sample 73Y at 83 ± 17 GPa, which are comprised from multiple tests, are reasonably close to previously documented properties. At present, it is not understood why the modulus value for the Zr failed specimen from sample 72Y is larger than the expected literature values. Considering that the single test specimen that failed due to localized plasticity in the Zr region of its gauge taken from the 72Y parent sample contains nominally 7-μm-wide by 9-μm-long by 7-μm-thick of Zr volume, perhaps an insufficient number of Zr grains in all possible orientations are being sampled to arrive at the bulk alpha Zr value. The adiabatic elastic moduli of single crystal alpha zirconium ranges from 32–165 GPa, as reported in [39]. Interestingly, the c11 orientation has a modulus of 143.6 GPa, which is 117% of our experimentally measured elastic modulus, 123 GPa. This suggests that the 72Y specimen that underwent deformation in its Zr region may contain a single grain or several grains close to the c11 orientation. More U-Mo/Zr tests that deform in their Zr regions would be required to produce better statistics more representative of the bulk modulus of alpha Zr. Because three specimens tested from 73Y failed due to localized plasticity in their Zr regions, it is speculated that the statistical average of these three tests is in good agreement with the bulk modulus of alpha Zr because a sufficient number of grains in all orientations are being sampled.

The strength of the specimens that failed in the Zr from both samples 72Y and 73Y are higher than would be expected for annealed Zr (389 MPa at thermal neutron fluence of 24.5×10^{19} n/cm^2). Recall that in the fabrication process, the cold-rolled foil with U-Mo and Zr layers is encapsulated in the Al and then HIPed to perform the final bonding. The HIP temperature is 833 K, which is lower than the 978 K considered necessary for annealing Zr (annealing temperature is 978 K per [38]). As a result, we can expect the Zr layer to retain some of the strength from cold working. Cold-worked and then irradiated Zr strength values have been published in [40] and were digitized and tabularized in [8]. From the strength values determined in this work, we can see that the strength of the Zr region of the gauge retains values consistent with between 20% and 50% cold work, 578 MPa and 665 MPa, at 24.5×10^{19} n/cm^2 neutron fluence, respectively.

The ultimate tensile strength of all tensile specimens from samples 72Y and 73Y that fractured within their U-Mo fuel regions were assessed via Weibull statistics. The results of the Weibull analysis are provided in Table 4. Following the methods outlined in Mauseth et al. [25], two-parameter Weibull statistics were employed to determine the distribution shape, analyze failure probability trends, and identify key metrics such as scale and shape parameters, as these materials are brittle and their tensile strength is influenced by flaws [41]. The Weibull shape parameter (β) was vital for accurately modeling the distribution of micro-tensile data, affecting the relationship between the mean, median, and mode of the strength distribution. In skewed distributions, the mean and mode differ significantly, while the median remains more centered between the two. Consequently, the Weibull median is a more reliable measure of UTS in the presence of outliers in a skewed distribution. Additionally, the coefficient of determination (R^2) was used to assess the goodness-of-fit of the Weibull model, indicating how well the model explains the variability of the data. The P-value provided a measure of the statistical significance of the model parameters, aiding in determining the reliability of the fit [42].

Despite variability in individual specimen strengths (Table 3), the data have a good fit with a Weibull distribution suggesting that scale effects are not negatively affecting the distribution of the results. This is important because Weibull weakest link theory predicts that larger specimens are more likely to contain a critical size flaw and thus fail at lower strengths.

Creating and testing micro-mechanical samples presents significant challenges, often resulting in smaller sample population sizes. Given this limitation, the results should be considered as guidelines rather than definitive conclusions. It is important to clearly state that the confidence level for this data is limited, and it should be interpreted with caution. Nonetheless, the Weibull approach remains the most effective method for analyzing strength distributions in irradiated micro-scale specimens.

Table 4. Ultimate tensile strength two-parameter Weibull Distribution values for specimens which failed in the U-Mo portion of the gauge.

Parameter	Value
Shape Parameter, β	7.07
R^2	0.93
P-Value	1.61E-05
Normal Mean UTS (MPa)	580.17
Weibull Mean UTS (MPa)	579.44
Normal Standard Deviation (MPa)	79.58
Weibull Standard Deviation (MPa)	96.43
Weibull Mode UTS (MPa)	605.90
Weibull Median UTS (MPa)	587.84

The Weibull probability density function is shown in Figure 11, and the Weibull survival function is shown in Figure 12.

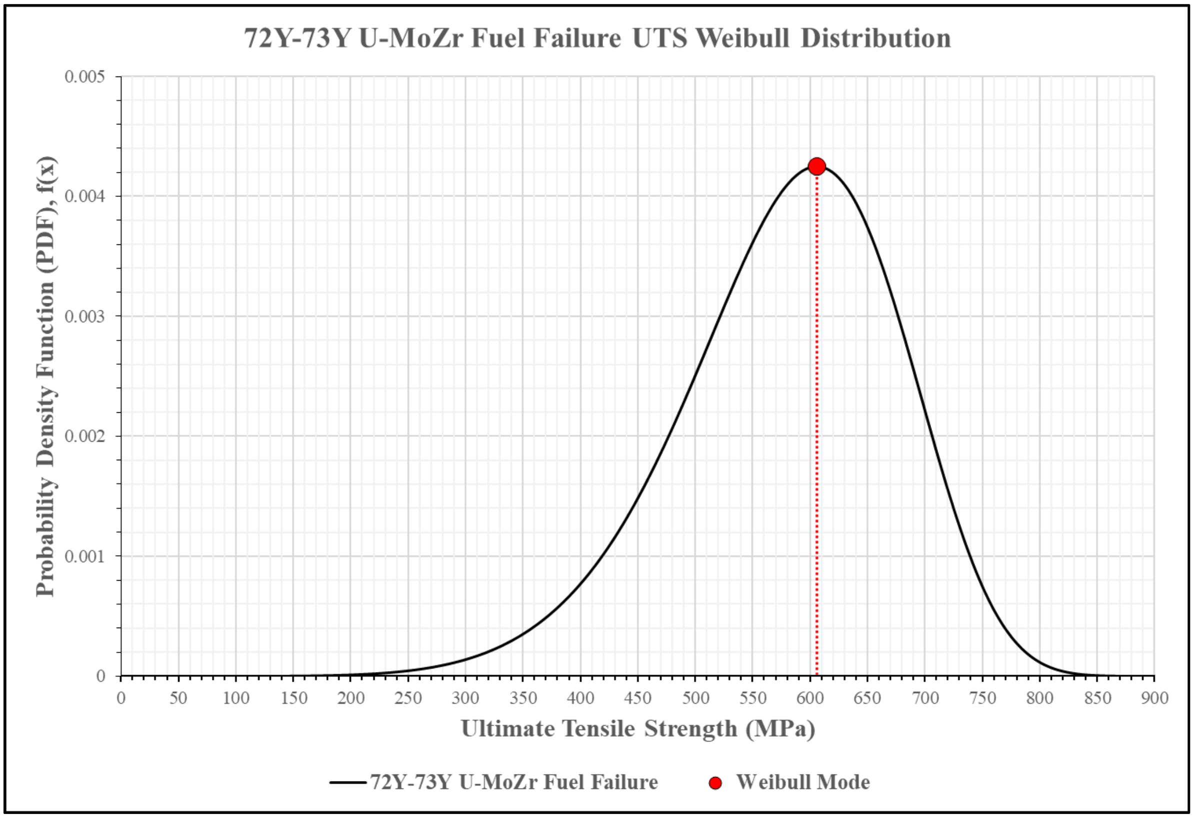

Figure 11. 72Y and 73Y U-Mo fuel failure probability density function of UTS Weibull Distribution.

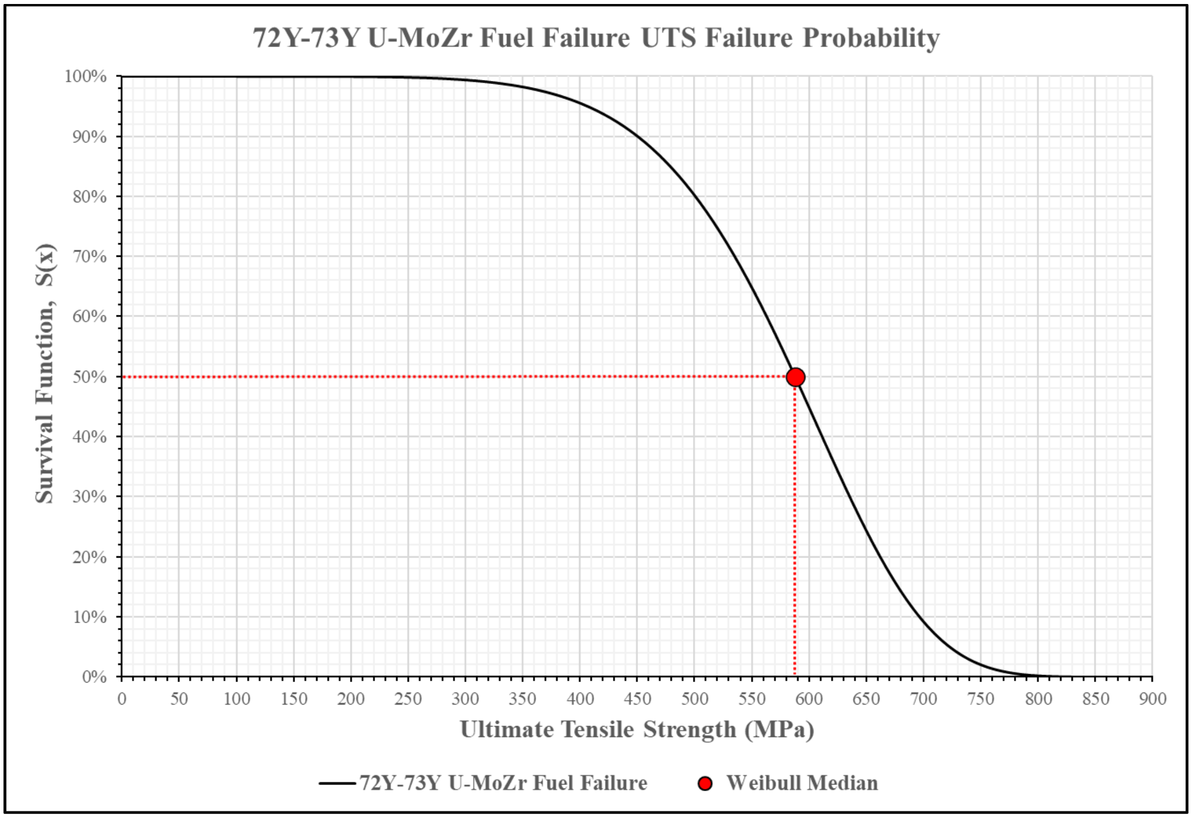

Figure 12. 72Y and 73Y U-Mo fuel failure survival function of UTS Weibull Distribution.

Conclusions

This study investigated the mechanical integrity of the diffusion bonds in monolithic plate-type nuclear fuel composed of a U-Mo alloy foil, Zr diffusion layer, and Al cladding, using a lift–out micro-tensile technique for specimens with approximate dimensions of 7 × 7 × 20 μm^3. Due to the geometric constraints of the parent material, this micro-mechanical testing is the only viable method of directly investigating the strength of the diffusion interfaces at intermediate burnups to ensure that adequate bond strength is established.

Materials were selected from the AFIP-7 neutron irradiation experiment, specifically where the local fission densities of 1.69×10^{21} fissions/cm^3 (73Y) and 2.0×10^{21} fissions/cm^3 (72Y). Results show that:

<u>Zr/Al diffusion bond</u>

All samples failed in the bulk aluminum, not at the diffusion bond. This indicates that the Zr/Al interface is stronger than the surrounding aluminum with measured properties of:

- Sample 72Y: Average yield strength = 125 ± 10 MPa, UTS = 156 ± 21 MPa, Strain at failure = 37.9 ± 5.6%
- Sample 73Y: Average yield strength = 139 ± 24 MPa, UTS = 185 ± 14 MPa, Strain at failure = 29.7 ± 3.4%

Zr/U-Mo bond

No samples failed in the diffusion zone.

- Some failed in the bulk Zr (ductile failure, high strain)
- Others failed in the U-Mo (brittle failure, low strain)
- Sample 73Y results were consistent with prior literature for both modulus and strength.
- Sample 72Y showed higher-than-expected modulus in U-Mo and Zr, possibly due to grain orientation effects.

72Y only produced one test in which the sample broke in the Zr portion of the gauge. For this single sample, the modulus was 123 GPa, larger than expected for bulk alpha Zr (93 GPa), presumably because a single grain or limited number of grains are being samples. The Zr orientation in this specimen is hypothesized to be oriented more closely to the c11 orientation of alpha Zr ($E_{c11\text{-}\alpha Zr}$ = 146.3 GPa). However, the modulus results from sample 73Y, which are averaged from multiple tests are reasonably close to bulk modulus values at 83 ± 17 GPa.

The specimens that failed in the U-Mo portion of the gauge were further analyzed via Weibull analysis due to the brittle nature of their failure. The results indicate a good fit with a Weibull distribution. It was further found that the results show a skewed distribution, meaning the Weibull median UTS is the more representative measure of ultimate tensile strength, which was found to be 587.84 MPa.

This detailed investigation offers valuable insights into the robustness and potential failure modes of the difficult to interrogate Al/Zr and Zr/U-Mo interfaces. These findings indicate that at the intermediate burnups investigated, the diffusion bond interfaces are stronger than the surrounding bulk material. Further testing at higher burnup levels is recommended to determine whether a transition in failure mode occurs as porosity and irradiation damage accumulate.

Acknowledgements

This work was supported through the U.S. Department of Energy National Nuclear Security Administration under the United States High-Performance Research Reactor Project and DOE Idaho Operations Office Contract DE-AC07-05ID14517. Accordingly, the U.S. Government retains and the publisher, by accepting the article for publication, acknowledges that the U.S. Government retains a nonexclusive, paid-up, irrevocable, world-wide license to publish or reproduce the published form of this manuscript, or allow others to do so, for U.S. Government purposes.

Declaration of Interest

This information was prepared as an account of work sponsored by an agency of the U.S. Government. Neither the U.S. Government nor any agency thereof, nor any of their employees, makes any warranty, express or implied, or assumes any legal liability or responsibility for the accuracy, completeness, or usefulness of any information, apparatus, product, or process disclosed, or represents that its use would not infringe privately owned rights. References herein to any specific commercial product, process, or service by trade name, trademark, manufacturer, or otherwise, does not necessarily constitute or imply its endorsement, recommendation, or favoring by the U.S. Government or any agency thereof. The views and opinions of authors expressed herein do not necessarily state or reflect those of the U.S. Government or any agency thereof.

References

[1] J. L. Snelgrove, G. L. Hofman, M. K. Meyer, C. L. Trybus, and T. C. Wiencek, "Development of very-high-density low-enriched-uranium fuels," *Nuclear Engineering and Design,* vol. 178, no. 1, pp. 119-126, 1997, doi: https://doi.org/10.1016/S0029-5493(97)00217-3.

[2] S. Van den Berghe, A. Leenaers, E. Koonen, and L. Sannen, "From High to Low Enriched Uranium Fuel in Research Reactors," *Advances in Science and Technology,* vol. 73, pp. 78–90, 2010, doi: https://doi.org/10.4028/www.scientific.net/ast.73.78.

[3] V. V. Joshi, E. A. Nyberg, C. A. Lavender, D. Paxton, and D. E. Burkes, "Thermomechanical process optimization of U-10wt% Mo – Part 2: The effect of homogenization on the mechanical properties and microstructure," *Journal of Nuclear Materials,* vol. 465, pp. 710-718, 2015, doi: 10.1016/j.jnucmat.2015.07.005.

[4] V. V. Joshi, E. A. Nyberg, C. A. Lavender, D. Paxton, H. Garmestani, and D. E. Burkes, "Thermomechanical process optimization of U-10 wt% Mo – Part 1: high-temperature compressive properties and microstructure," *Journal of Nuclear Materials,* vol. 465, pp. 805-813, 2015, doi: 10.1016/j.jnucmat.2013.10.065.

[5] Y. Park *et al.*, "Growth kinetics and microstructural evolution during hot isostatic pressing of U-10 wt.% Mo monolithic fuel plate in AA6061 cladding with Zr diffusion barrier," *Journal of Nuclear Materials,* vol. 447, no. 1-3, pp. 215-224, 2014, doi: **https://doi.org/10.1016/j.jnucmat.2014.01.018**.

[6] E. Perez, D. D. Keiser, and Y. H. Sohn, "Phase Constituents and Microstructure of Interaction Layer Formed in U-Mo Alloys vs Al Diffusion Couples Annealed at 873 K (600 °C)," *Metallurgical and Materials Transactions A,* vol. 42, no. 10, pp. 3071-3083, 2011/10/01 2011, doi: 10.1007/s11661-011-0733-9.

[7] E. Perez, B. Yao, D. D. Keiser, and Y. H. Sohn, "Microstructural analysis of as-processed U–10wt.%Mo monolithic fuel plate in AA6061 matrix with Zr diffusion barrier," *Journal of Nuclear Materials,* vol. 402, no. 1, pp. 8-14, 2010/07/01/ 2010, doi: https://doi.org/10.1016/j.jnucmat.2010.04.016.

[8] B. Rabin *et al.*, "Preliminary Report on U-Mo Monolithic Fuel for Research Reactors Rev 4," Idaho National Laboratory, Idaho Falls, Idaho, USA, INL/EXT-17-40975, 2020.

[9] M. K. Meyer *et al.*, "IRRADIATION PERFORMANCE OF U-Mo MONOLITHIC FUEL," *Nuclear Engineering and Technology,* vol. 46, no. 2, pp. 169-182, 2014/04/01/ 2014, doi: https://doi.org/10.5516/NET.07.2014.706.

[10] K. Farrell, "A SPECTRAL EFFECT ON PHASE EVOLUTION IN NEUTRON-IRRADIATED ALUMINUM?*," in "Mat. Res. Soc. Symp. Proc," 1995, vol. 373. [Online]. Available: https://link.springer.com/article/10.1557/PROC-373-165

[11] K. Farrell, "5.07 Performance of Aluminum in Research Reactors," *Comprehensive Nuclear Materials,* vol. 5, pp. 143-175, 2012, doi: https://doi.org/10.1016/B978-0-08-056033-5.00113-0.

[12] K. Farrell and R. T. King, *Tensile Properties of Neutron-Irradiated 6061 Aluminum Alloy in Annealed and Precipitation-Hardened Conditions* (ASTM STP 683 Effects of Radiation on Structural Materials). Richland: American Society for Testing and Materials, 1979, pp. 440-449.

[13] K. Farrell, J. O. Stiegler, and R. E. Gehlbach, "Metallography Transmutation-Produced Silicon Precipitates in Irradiated Aluminum a," 1970. [Online]. Available: https://www.sciencedirect.com/science/article/pii/0026080070900157

[14] J. Schulthess *et al.*, "Mechanical and Thermophysical properties of low enriched uranium-10wt% molybdenum rolled foils," *Journal of Nuclear Materials,* vol. 563, p. 153628, 2022, doi: 10.1016/j.jnucmat.2022.153628.

[15] J. Schulthess, R. Lloyd, B. Rabin, M. Heighes, T. Trowbridge, and E. Perez, "Elevated temperature tensile tests on DU–10Mo rolled foils," *Journal of Nuclear Materials,* vol. 510, pp. 282-296, 2018, doi: 10.1016/j.jnucmat.2018.08.024.

[16] J. L. Schulthess *et al.*, "Mechanical Properties of Irradiated U-10 wt. %Mo Alloy Degraded by Porosity Development," *Journal of Nuclear Engineering and Radiation Science,* vol. 10, no. 3, 2024, doi: 10.1115/1.4064779.

[17] J. L. Schulthess, W. R. Lloyd, B. Rabin, K. Wheeler, and T. W. Walters, "Mechanical properties of irradiated U Mo alloy fuel," *Journal of Nuclear Materials,* vol. 515, pp. 91-106, 2019, doi: 10.1016/j.jnucmat.2018.12.025.

[18] W. Mohamed, H. Ozaltun, and H. S. Roh, "Summary of Property-Related Parameters and Its Efffect on the Simulated Thermo-Mechanical Behavior of U-10Mo Monolithic Fuel Plate," in *ASME 2022 Power Conference*, Pittsburgh, PA, 2022: ASME, doi: 10.1115/power2022-86012. [Online]. Available: https://dx.doi.org/10.1115/power2022-86012

[19] H. Ozaltun, "Evaluation of Interface Stresses and Cladding-Cladding Delamination Failures In U-Mo Fuel Plates," *International Conference on Nuclear Engineering, Proceedings, ICONE,* vol. 2, 2021/10// 2021, doi: 10.1115/ICONE28-65840.

[20] H. Ozaltun, M. H. Herman Shen, and P. Medvedev, "Assessment of residual stresses on U10Mo alloy based monolithic mini-plates during Hot Isostatic Pressing," *Journal of Nuclear Materials,* vol. 419, no. 1-3, pp. 76-84, 2011/12// 2011, doi: 10.1016/J.JNUCMAT.2011.08.029.

[21] H. Ozaltun and S. J. Miller, "Evaluation of Blister Behavior for U10Mo Mini Fuel Plates With Cold Rolled Foils," in *Proceedings of the ASME 2012 International Mechanical Engineering Congress and Exposition*, Houston, Texas, USA, 2012, vol. Volume 6: Energy, Parts A and B: American Society of Mechanical Engineers, pp. 1337-1345, doi: https://doi.org/10.1115/IMECE2012-93141.

[22] H. Ozaltun, H. S. Roh, and W. Mohamed, "Overview of the base model for the parametric sensitivity studies specific to performance assessments of U-Mo fuel plates," in *ASME International Mechanical Engineering Congress and Exposition*, 2022: ASME. [Online]. Available: https://doi.org/10.1115/IMECE2022-FM1. [Online]. Available: https://doi.org/10.1115/IMECE2022-FM1

[23] D. Frazer, D. Jadernas, N. Bolender, J. Madden, J. Giglio, and P. Hosemann, "Elevated temperature microcantilever testing of fresh U-10Mo fuel," *Journal of Nuclear Materials,* vol. 526, 2019, Art no. 151746, doi: https://doi.org/10.1016/j.jnucmat.2019.151746.

[24] D. Frazer *et al.*, "Micro-tensile testing of the bond line in hot isostatic pressed aluminum," *Journal of Nuclear Materials,* vol. 561, p. 153532, 2022/04/01/ 2022, doi: https://doi.org/10.1016/j.jnucmat.2022.153532.

[25] T. Mauseth, M. L. Dunzik-Gougar, S. Meher, and I. J. van Rooyen, "Determining the tensile strength of fuel surrogate TRISO-coated particle buffer, IPyC, and buffer-IPyC interlayer regions," *Journal of Nuclear Materials,* vol. 583, p. 154540, 2023/09/01/ 2023, doi: https://doi.org/10.1016/j.jnucmat.2023.154540.

[26] D. J. Edwards *et al.*, "Characterization of U-Mo Foils for AFIP-7," Pacific Northwest National Laboratory, Richland, WA, USA, PNNL-21990, 2012. [Online]. Available: https://www.pnnl.gov/publications/characterization-u-mo-foils-afip-7
[27] G. Moore, "AFIP-7 Fabrication Summary Report," Idaho National Laboratory, Idaho Falls, ID, USA, INL/LTD-12-26917, 2012.
[28] D. M. Perez, J. W. Nielsen, G. S. Chang, G. A. Roth, and N. E. Woolstenhulme, "AFIP-7 Irradiation Summary Report," Idaho National Laboratory, Idaho Falls, Idaho, USA, INL/EXT-12-25915, 2012. [Online]. Available: https://www.osti.gov/servlets/purl/1083244
[29] A. B. Robinson *et al.*, "AFIP-7 Post-irradiation Examination Summary Report," United States, 21 2016. [Online]. Available: https://www.osti.gov/biblio/2478498

https://www.osti.gov/servlets/purl/2478498
[30] W. J. Williams, A. B. Robinson, and B. H. Rabin, "Post-Irradiation Non-Destructive Analyses of the AFIP-7 Experiment," *JOM,* vol. 69, no. 12, pp. 2546-2553, 2017/12/01 2017, doi: 10.1007/s11837-017-2552-y.
[31] *ASTM B209-14 Standard Specification for Aluminum and Aluminum-Alloy Sheet and Plate*, ASTM B209-14, 2021. [Online]. Available: https://www.astm.org/standards/b209
[32] *Heat Treating of Aluminum Alloys*. ASM International, 1991.
[33] P. Hosemann, "Small-scale mechanical testing on nuclear materials: bridging the experimental length-scale gap," *Scripta Materialia,* vol. 143, pp. 161-168, 2018/01/15/ 2018, doi: https://doi.org/10.1016/j.scriptamat.2017.04.026.
[34] P. Hosemann and J. G. Gigax, "Short-Pulsed Laser Techniques for Materials Modification, Characterization, and Synthesis," *JOM,* vol. 73, no. 12, pp. 4209-4210, 2021/12/01 2021, doi: https://doi.org/10.1007/s11837-021-04975-6.
[35] L. Li *et al.*, "Empirical validation of size effects in sub-sized tensile specimens for nuclear structural materials," *Scientific Reports,* vol. 15, no. 1, p. 13846, 2025/04/22 2025, doi: 10.1038/s41598-025-98849-5.
[36] J. Schulthess, "Elevated Temperature Tensile Tests on {DU}{\textendash}10Mo Rolled Foils," 2014 2014.
[37] D. Leguillon, É. Martin, and M.-C. Lafarie-Frenot, "Flexural vs. tensile strength in brittle materials," *Comptes Rendus Mécanique,* vol. 343, no. 4, pp. 275-281, 2015, doi: 10.1016/j.crme.2015.02.003.
[38] A. S. M. H. Committee, *Properties and Selection: Nonferrous Alloys and Special-Purpose Materials*: ASM International, 1990. [Online]. Available: https://doi.org/10.31399/asm.hb.v02.9781627081627.
[39] E. S. Fisher and C. J. Renken, "Adiabatic elastic moduli of single crystal alpha zirconium," *Journal of Nuclear Materials,* vol. 4, no. 3, pp. 311-315, 1961/08/01/ 1961, doi: https://doi.org/10.1016/0022-3115(61)90081-2.
[40] "Zirconium - Its Production and Properties," in "USBM Bulletin," U.S. Bureau of Mines, 561, 1956.
[41] D. P. H. Hasselman, "Griffith flaws and the effect of porosity on tensile strength of brittle ceramics," *Journal of the American Ceramic Society,* vol. 52, no. 8, pp. 457-457, 1969.
[42] H. Rinne, *The Weibull distribution: a handbook*. Chapman and Hall/CRC, 2008.